Chapter 6

The Future of Soil Micromorphology

File 76: The Future of Soil Micromorphology

The advancement of technology opens up new opportunities to soil micromorphology. Although a description using an optical microscope of the fabric and the various constituents of soils will be always necessary to investigate soil evolution, the uncovered thin section leaves soil material on which analyses can be performed. Since the 1970s, it was possible to observe thin sections at high resolution with the scanning electron microscope in its backscattered electron mode (see "File 7"). It was also possible to generate chemical images with electron microprobes. But these conventional techniques, as well as new ones, greatly improve the study of matter interactions in soils, not only by enhancing the spatial resolution with incredible precision but also by providing chemical and mineralogical images, which substantially increased the accuracy of micromorphological diagnostics. By coupling morphological and chemical approaches, including stable isotope imaging in soil material, the future of soil micromorphology will undoubtedly offer new opportunities to solve specific problems, especially in the field of organomineral interactions in soils. It is wise to say that soil micromorphology, with its analytical and holistic approaches, will make it possible to build the necessary solid foundations needed for investigations that are increasingly oriented towards nanoscale objects: it will remind us that the trees should not hide the forest.

Cockpit of the microXAS Beamline at the Swiss Light Source, Paul Scherrer Institute, Villigen PSI, Switzerland.

E. P. Verrecchia, L. Trombino, *A Visual Atlas for Soil Micromorphologists*,
https://doi.org/10.1007/978-3-030-67806-7_6

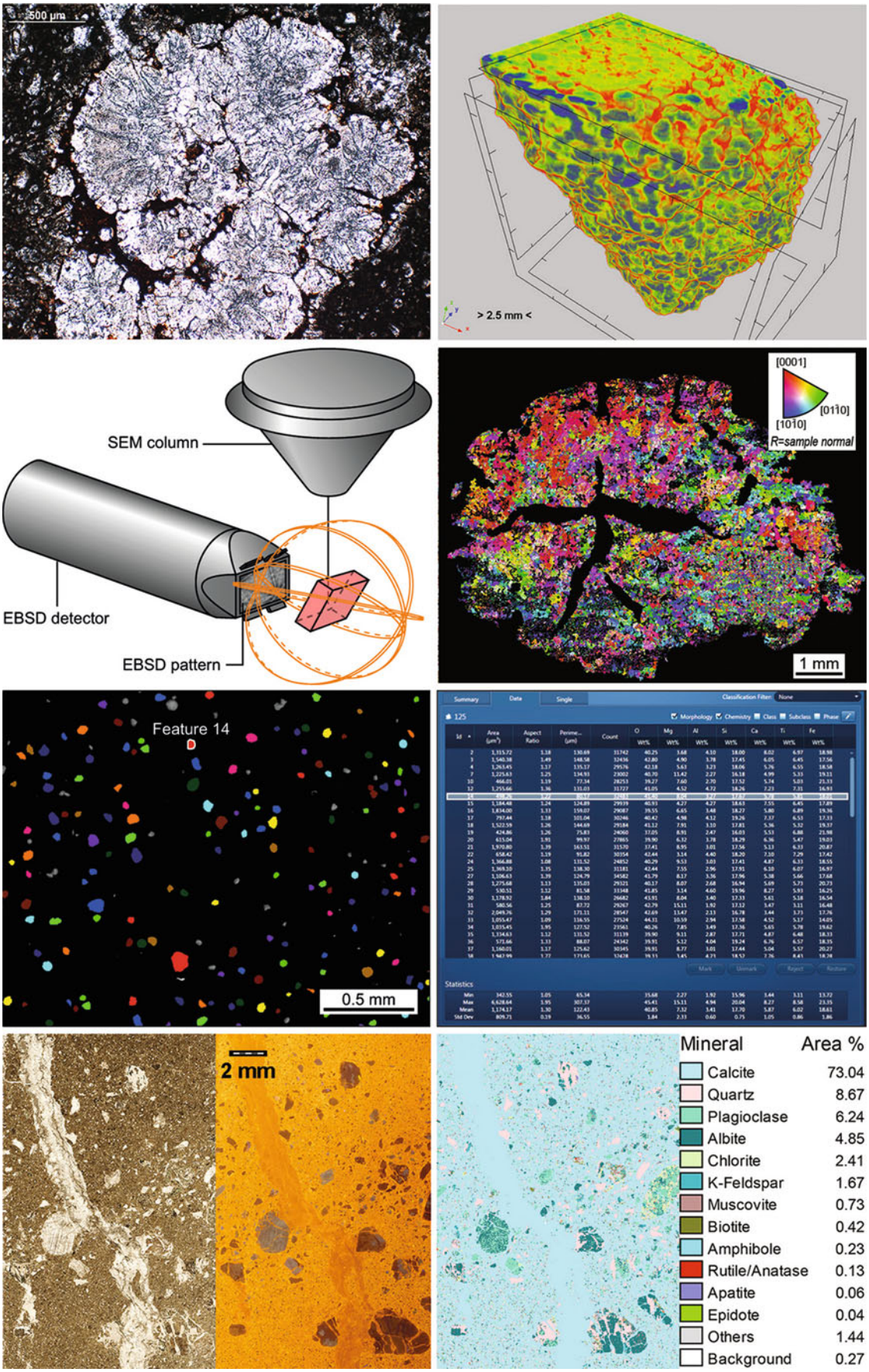
500 µm
> 2.5 mm <
SEM column
EBSD detector
EBSD pattern
[0001]
[01$\bar{1}$0]
[10$\bar{1}$0]
R=sample normal
1 mm
Feature 14
0.5 mm
2 mm
Mineral
Area %
Calcite 73.04
Quartz 8.67
Plagioclase 6.24
Albite 4.85
Chlorite 2.41
K-Feldspar 1.67
Muscovite 0.73
Biotite 0.42
Amphibole 0.23
Rutile/Anatase 0.13
Apatite 0.06
Epidote 0.04
Others 1.44
Background 0.27

File 77: Beyond the Two Dimensions

Based on density variation and X-ray attenuation, X-ray microtomography makes it possible to visualize the organization of voids and particles of different natures in a soil volume. Another tool, electron backscatter diffraction (EBSD), can be used to detect the crystallographic axes of minerals in a thin section of soil. Finally, a device such as the QEMSCAN opens the avenue of quantitative analysis of minerals in thin sections of soil.

Captions from upper left corner to lower right corner.

1. View in PPL of *Microcodium* in a paleosol from the Corbières, southern France.
2. Soil 3D-block at the same location as 1. observed with a high energy micro-CT scanner. This instrument produces a three-dimensional X-ray attenuation map for rock or soil samples in a non-destructive way. In this case, it is possible to see that *Microcodiums* form a dense and intertwined mesh of biominerals.
3. Sketch showing the generation of an EBSD Kikuchi pattern from the interaction between the SEM electron beam and the sample's crystal lattice. Within the sample, elastic and inelastic scattering produces a three-dimensional interaction volume of multidirectional electrons. When the Bragg conditions are satisfied, constructive interference occurs, generating straight and parallel line pairs when projected onto the EBSD detector screen. The association of bands forms an EBSD Kikuchi pattern from which the crystallographic orientation of the material can be determined. Courtesy of Dr. Pierre Vonlanthen (University of Lausanne).
4. EBSD inverse pole figure map of a calcite nodule (Cameroon) showing orientations of calcite crystallographic axes with respect to a reference sample. Here, pixels coloured in red are those for which calcite [0001] axes are (closely) parallel to the sample normal. The occurrence of nearby grains with similar colours indicates a non-random distribution of crystallographic orientations. For a detailed review of the EBSD technique, see Prior et al. (1999) or Schwarzer et al. (2009).
5. Automatic morphological and chemical analyses of soil particles performed in the SEM using the AZtec Feature software plug-in by Oxford Instruments. Particles are detected in the backscattered electron image based on greyscale levels and site-specifically analysed for chemistry using X-ray energy-dispersive spectroscopy.
6. Lookup table listing the morphological parameters and elemental composition corresponding to each individual particle.
7. PPL (left) and cathodoluminescence views of a carbonate-rich thin section.
8. QEMSCAN image of the same view as 7. showing the distribution of the various minerals detected and their relative proportions. Calcite dominates the mineral fraction of this thin section, followed by quartz and plagioclase. Courtesy of Dr. Kalin Kouzmanov (University of Geneva).

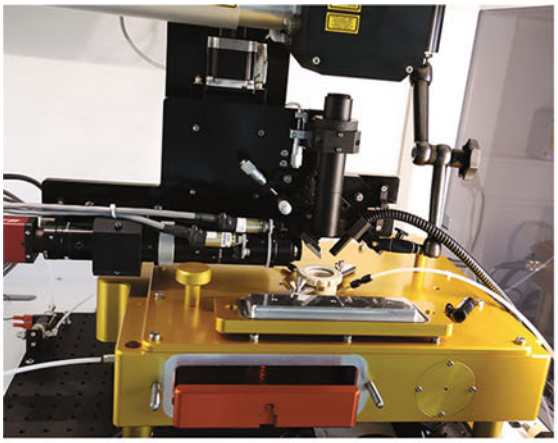

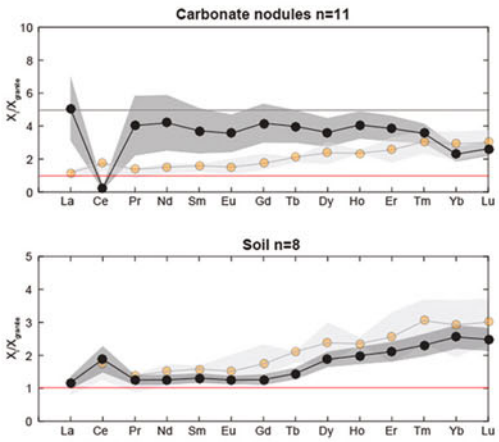
Carbonate nodules n=11
La Ce Pr Nd Sm Eu Gd Tb Dy Ho Er Tm Yb Lu

Soil n=8
La Ce Pr Nd Sm Eu Gd Tb Dy Ho Er Tm Yb Lu

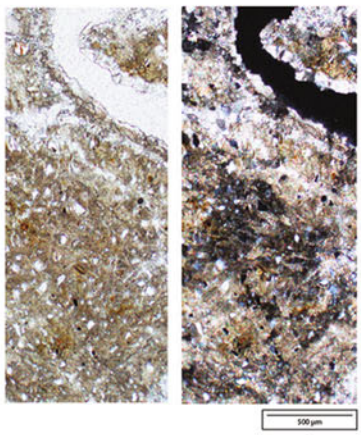

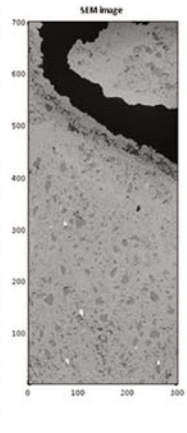
SEM image

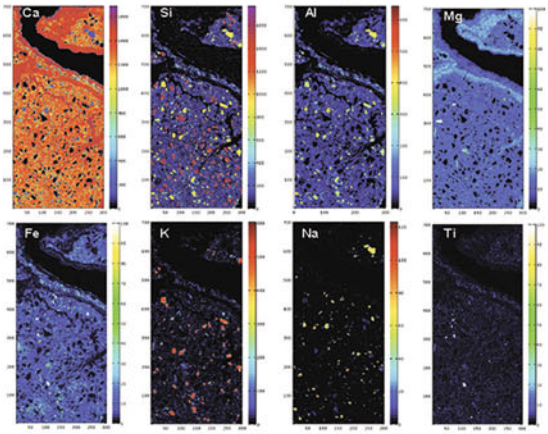
Ca
Si
Al
Mg
Fe
K
Na
Ti

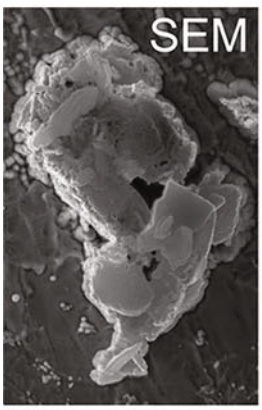
SEM

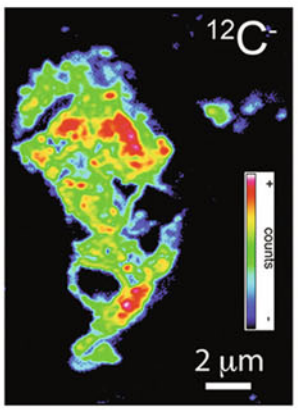
12C-
counts
2 µm

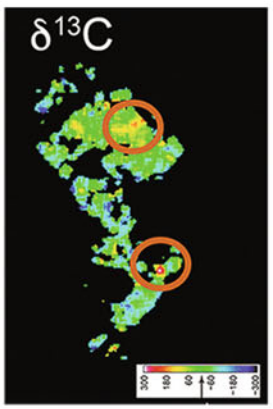
δ13C

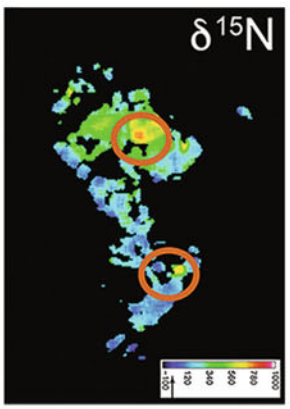
δ15N

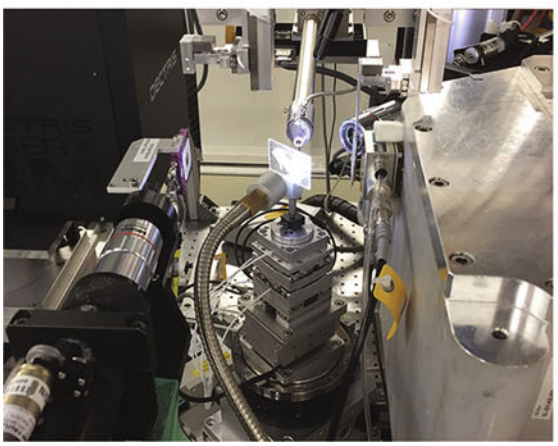

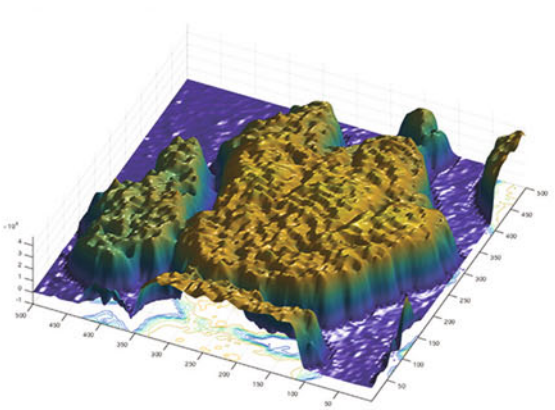

File 78: The Prospect of Chemical Imaging

It must not be forgotten that uncovered thin sections are still a natural soil sample. Minerals and organic matter remain accessible for measurements, and this is particularly true with modern instruments, with which it is possible to map the chemical and mineralogical compositions of the various components forming the soil. This section provides a few examples of chemical measurements made on sections or small soil objects, performed with different instruments.

Captions from upper left corner to lower right corner.

1. S155 two-volume ablation cell of a RESOlution ablation system. A sample shuttle for custom-sized samples (in red) is partly inserted in the cell (in yellow). The ablated aerosol is extracted through the extraction funnel in the central part of the cell and directed towards the torch of the ICP-MS, where the ablated particles are heated and vaporized, and the chemical elements contained in them, ionized. Courtesy of Dr. Alexey Ulyanov (University of Lausanne).
2. Comparison of REE average distributions in carbonate nodules ($n = 11$; upper curve in black) and soils ($n = 8$; lower curve in black) with respect to Saharan dust (in orange). Dark grey shaded area refers to (1σ) standard deviation. Paleo-Vertisols from northern Cameroon (Dietrich et al. 2017). The REE abundance has been directly measured by laser-ablation ICP-MS with the instrument shown partially in photograph 1.
3. PPL, XPL, and scanning electron microscope in backscattered electron mode views of a carbonate nodule from a Vertisol (Cameroon).
4. Distribution maps of elements (Ca, Si, Al, Mg, Fe, K, Na, and Ti) obtained using wavelength-dispersive X-ray spectroscopy of the same sample as in 3. Warmer colours refer to relatively higher contents. Courtesy of Dr. Nathalie Diaz (University of Lausanne).

5.–6. NanoSIMS images of glycine-derived ^{13}C and ^{15}N spots identified at the surface of soil aggregates, randomly isolated from soil density fractions, separated from a surface forest soil, and incubated for 8 h with uniformly $^{13}C/^{15}N$-labelled glycine (Hatton et al. 2015). The arrow represents the natural values for ^{13}C and ^{15}N isotope ratios. Courtesy of Dr. Laurent Remusat (Muséum National d'Histoire Naturelle, France).

7. Thin section (bright light in the centre) placed under the microXAS beamline at the Swiss Light Source, Paul Scherrer Institute, Villigen PSI, Switzerland.
8. Map of cryptomelane distribution (low content in blue, high content in yellow) inside a digitate manganese nodule observed in a soil developed on travertine, Morocco. The nodule is approximately 100 µm in width.